Journal of Sound and Vibration 326 (2009) 213–220

Contents lists available at ScienceDirect

Journal of Sound and Vibration

journal homepage: www.elsevier.com/locate/jsvi

Piezoelectric generation of extensional waves in an elastic bar by use of a power amplifier with constrained output current

A. Jansson, B. Lundberg *

The Ångström Laboratory, Uppsala University, Box 534, SE-751 21 Uppsala, Sweden

ARTICLE INFO

Article history:
Received 17 July 2008
Received in revised form
6 March 2009
Accepted 11 April 2009
Handling Editor: A.V. Metrikine
Available online 20 May 2009

ABSTRACT

Generation of extensional waves in a linearly elastic bar by means of a pair of attached piezoelectric actuators driven by a power amplifier with output current constraints is studied theoretically and experimentally. In addition to its current constraints, the amplifier is characterized by its DC voltage gain and 3 dB cut-off frequency. On the basis of 1D wave propagation, time-domain relations are established for the nonlinear dependence of the output voltage and current of the amplifier, and of the strain associated with the waves generated, on the input voltage. It is found that the amplifier model used allows prediction of the main features of this dependence. Nonlinear operation due to constrained output current may occur even at a low input voltage if the rate of change of this voltage is excessive. Consideration of this phenomenon is important in, e.g., control applications.

1. Introduction

Piezoelectric plates covered by electrode surface layers are increasingly used as actuators in structural, space, medical and other applications. An actuator of this type, driven by a power amplifier, can be used for generation of transient waves in a structure. If there is a known relation between the waves generated and the input voltage of the amplifier, waves of prescribed shapes can be generated. This is of importance in, e.g., control applications [1].

The relation between waves generated and input voltage is simple if the amplifier operates linearly and its output impedance can be neglected in comparison with the input impedance of the actuator/structure assembly. In this case, the output voltage can be determined without considering the output current. This implies that the piezoelectric material can be characterized by a single constitutive relation, the actuator equation, which relates strain to stress and electric field strength. Due to constraints on output current, however, the amplifier operation is not always linear. Such constraints are normally introduced as a transistor protection against excessive input, output short-circuit, etc. Furthermore, the output impedance cannot always be neglected. In each of these situations, the output voltage cannot be determined without considering the output current. This requires the involvement of a second constitutive relation, the sensor equation, which relates electric displacement to stress and electric field strength.

Early work on the interaction of piezoelectric actuators and an Euler–Bernoulli beam was carried out by Crawley and de Luis [2]. The dynamics of the actuator was taken into account by, e.g., Pan et al. [3] who studied an Euler–Bernoulli beam with attached piezoelectric actuators. Allowance for the interaction of structure and electrical circuits, and for the two

* Corresponding author.
E-mail address: bengt.lundberg@angstrom.uu.se (B. Lundberg).

0022-460X/$ - see front matter © 2009 Elsevier Ltd. All rights reserved.
doi:10.1016/j.jsv.2009.04.017

Nomenclature

Latin

a	distance
A	cross-sectional area
c	wave speed
C	capacitance
d	piezoelectric constant
e	strain
E	Young's modulus
G	voltage gain of unloaded amplifier
h	height
i	current
k	square root of piezoelectric coupling coefficient
K	stiffness
l	length
L	inductance
N	normal force
R	resistance
t	time
U	voltage
v	particle velocity
w	width
x	axial coordinate
y	transverse coordinate (horizontal)
z	transverse coordinate (vertical)
Z	impedance (mechanical, electrical, or mixed)

Greek

γ	wave propagation coefficient
ε	permittivity
ρ	density
ω	angular frequency

Superscripts

0	low-frequency limit
E	electrical
M	mechanical

Subscripts

0	electrical port
1, 2	1st and 2nd mechanical ports
a	piezoelectric actuator
c	core layer, constraint
ch	characteristic
cut	cut-off
G	generated
int	internal
s	source
tr	transit

coupled constitutive equations, was made, e.g., by Hagood et al. [4], Thornburgh and Chattopadhyay [5], and Thornburgh et al. [6]. The dynamics of the amplifier was considered by, e.g., Niezrecki and Cudney [7] and Leo [8].

Generation of extensional waves in a linearly elastic or viscoelastic bar by means of a pair of piezoelectric actuators driven by a power amplifier operating linearly, without current constraint, has been investigated theoretically and experimentally by the authors in previous studies [9–11]. In the theoretical analyses, carried out essentially in the frequency domain, the output impedance was allowed to be finite, which required the use of both constitutive equations. In the experiments, aimed at generation of prescribed strain waves, precautions were taken to ensure linear operation. This was done by avoiding high rates of change of the input voltage.

Here, similar wave generation is studied theoretically and experimentally for a power amplifier operating nonlinearly due to output current constraints. Therefore, both constitutive equations must be taken into account in this study as well. As the effect of nonlinearity is much stronger than that of finite output impedance for the amplifier and actuator/bar assembly used, the output impedance is taken to be zero in the theoretical analysis, which is carried out essentially in the time domain. In particular, the responses in output voltage, output current, and strain generated in the bar to a step input voltage are studied. For such input, with a rapid change of the input voltage, the amplifier operates nonlinearly even at very low input voltages. The theoretical basis is given in Section 2, and the experimental tests are presented in Section 3. The results are presented and discussed in Section 4, and the main conclusions are given in Section 5.

2. Bar and actuators

Consider the electromechanical system in Fig. 1(a) consisting of a long linearly elastic bar with a pair of attached piezoelectric actuators a, electrically in parallel. The length of the laminated region $-l/2<x<l/2$ is l, where x is an axial coordinate as shown. This region is referred to as the piezoelectric bar element (PBE) [11]. A voltage $\hat{U}_0(\omega)$ from a power amplifier applied to the actuators results in a current $\hat{i}_0(\omega)$ and in the generation of outwards propagating extensional waves (G) in the bar. These waves are associated with the normal force $\hat{N}_G(\omega)$ and the velocity $\hat{v}_G(\omega)$ at the interfaces $x=\pm l/2$ as shown in Fig. 1(b). Here, ω is the angular frequency and $\hat{\phi}(\omega)$ denotes the Fourier transform of the function $\phi(t)$ of time t.

Thin bonding layers are assumed to perfectly attach the actuators to the bar. The cross-sections of the bar and the actuators are rectangular, and the full cross-sections inside and outside the PBE are symmetric with respect to the axes y and z. Outside the PBE, the bar has height h_1, width w_1 and cross-sectional area $A_1=h_1w_1$. In the core c of the PBE, it has

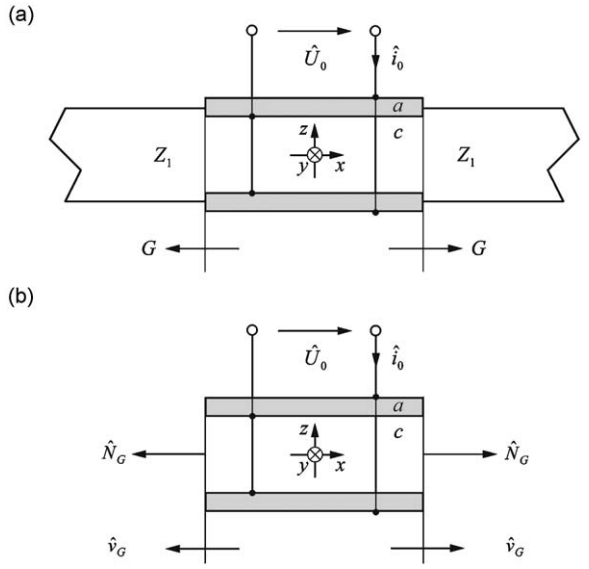

Fig. 1. Electromechanical system: (a) elastic bar with attached piezoelectric members and (b) three-port representation of laminated PBE.

height h_c, width w_c and cross-sectional area $A_c = h_c w_c$. Each actuator has height h_a, width w_a and cross-sectional area $A_a = h_a w_a$. Therefore, the total cross-sectional area is $A = 2A_a + A_c$ within the PBE.

The Young's modulus of the bar material is E_1, while the closed-circuit Young's modulus of the actuators is E_a. The densities are ρ_1 and ρ_a, respectively. It is assumed that initially plane cross-sections remain plane and that the stress is uni-axial in the x direction. Thus, within the PBE the effective Young's modulus is $E = (2A_a E_a + A_c E_c)/A$ with $E_c = E_1$, and the effective density is $\rho = (2A_a\rho_a + A_c\rho_c)/A$ with $\rho_c = \rho_1$. In the bar and the PBE the wave speeds are $c_1 = (E_1/\rho_1)^{1/2}$ and $c = (E/\rho)^{1/2}$, and the characteristic impedances are $Z_1 = A_1 E_1/c_1$ and $Z_{ch}^M = AE/c$, respectively.

The piezoelectric material, polarized in the z direction, is assumed to have linear electromechanical response. In addition to the closed-circuit Young's modulus E_a, this response is characterized by the permittivity ε_a and the piezoelectric constant $d_a = -d_{31}$. The electrical fields between the electrodes are assumed to be parallel to the z axis, and the effects of strains in the directions y and z are neglected.

3. Dynamics of PBE–bar assembly

The PBE is viewed as a three-port system with one electrical and two mechanical ports. It interacts with the external parts of the bar at the ports constituted by its ends as illustrated. Because of linearity, the generalized forces $\hat{U}_0, \hat{N}_G, \hat{N}_G$ are related to the generalized velocities $\hat{i}_0, \hat{v}_G, \hat{v}_G$ by an impedance matrix $\mathbf{Z}$ with elements $Z_{00}(\omega), Z_{01}(\omega), \ldots, Z_{22}(\omega)$ [11]. Due to reciprocity and the symmetry with respect to the yz plane, the impedance matrix is defined by the four independent elements $Z_{00}, Z_{01}(= Z_{10} = Z_{02} = Z_{20}), Z_{11}(= Z_{22})$ and $Z_{12}(= Z_{21})$. Here, these elements are [11]

$$Z_{00} = \frac{1}{2}\frac{Z_a^E}{1-k_a^2}, \quad Z_{01} = \frac{d_a h_a}{\varepsilon_a A_a}\frac{Z_a^M}{1-k_a^2} = A_a E_a \frac{d_a}{h_a}\frac{Z_a^E}{1-k_a^2},$$
$$Z_{11} = 2\frac{k_a^2 Z_a^M}{1-k_a^2} + \frac{Z_{ch}^M}{\tanh(\gamma l)}, \quad Z_{12} = 2\frac{k_a^2 Z_a^M}{1-k_a^2} + \frac{Z_{ch}^M}{\sinh(\gamma l)}, \tag{1}$$

where $Z_a^E = 1/\mathrm{i}\omega C_a$ is the electrical impedance of a single mechanically unloaded actuator with capacitance $C_a = \varepsilon_a w_a l/h_a$, $Z_a^M = K_a/\mathrm{i}\omega$ is the quasi-static mechanical impedance of a single closed-circuit actuator with stiffness $K_a = A_a E_a/l$, $k_a^2 = d_a^2 E_a/\varepsilon_a$ is the piezoelectric coupling coefficient, and $\gamma = \mathrm{i}\omega/c$ is the wave propagation coefficient in the PBE.

Continuity of force and velocity at the mechanical ports requires that $\hat{v}_G = -(1/Z_1)\hat{N}_G$. This equation and the two equations provided by the matrix relation between generalized forces and velocities constitute three equations for the three unknowns $\hat{i}_0$, $\hat{v}_G$ and $\hat{N}_G$. Solving for $\hat{i}_0$ and $\hat{N}_G$, and introducing the strain $\hat{e}_G = \hat{N}_G/Z_1 c_1$, gives [11]

$$\hat{i}_0 = \frac{\hat{U}_0}{Z_{\mathrm{int}}^E}, \tag{2}$$

$$\hat{e}_G = \frac{1}{c_1}\frac{Z_{01}}{Z_{00}(Z_{11}+Z_{12}+Z_1) - 2Z_{01}^2}\hat{U}_0, \tag{3}$$

where

$$Z_{\text{int}}^{E} = Z_{00} - \frac{2Z_{01}^2}{Z_{11} + Z_{12} + Z_1} \tag{4}$$

is the internal impedance of the PBE–bar assembly.

4. Dynamics of current-constrained power amplifier

An equivalent circuit of the power amplifier loaded by the internal impedance Z_{int}^{E} of the PBE–bar assembly is shown in Fig. 2. It is defined by its voltage gain $G(\omega)$ unloaded, its output impedance $Z_0(\omega)$ and its output current constraint $i_{\min} \leqslant i_0(t) \leqslant i_{\max}$. In what follows, the magnitude of the output impedance Z_0 of the amplifier will be neglected in comparison with that of the internal impedance Z_{int}^{E}, i.e., Z_0 will be taken as zero. This simplification is justified by the results of Ref. [10].

The input voltage $\hat{U}(\omega)$ of the amplifier produces the voltage

$$\hat{U}_s(\omega) = G(\omega)\hat{U}(\omega) \tag{5}$$

of an ideal internal source, where the voltage gain is taken as

$$G = \frac{G^0}{1 + \mathrm{i}\omega/\omega_{\text{cut}}}. \tag{6}$$

Here, G^0 is the DC voltage gain and ω_{cut} is the cut-off angular frequency of the unloaded amplifier.

With $Z_0 = 0$, as assumed, the output voltage and current of the amplifier are

$$U_0(t) = U_s(t), \quad i_{\min} < i_0(t) < i_{\max}, \tag{7}$$

$$U_0(t) = U_s(t) - U_c(t), \quad i_0(t) = i_{\max} \text{ or } i_{\min}. \tag{8}$$

Transitions from linear to current-constrained regimes occur when $i_0(t)$ becomes equal to $i_{\max}$ or $i_{\min}$, while transitions in opposite directions occur when $U_c(t)$ becomes zero.

5. Wave generation

Because of the nonlinear relation between the output voltage $U_0(t)$ and the output current $i_0(t)$ of the amplifier expressed by Eqs. (7) and (8), Eqs. (5), (2) and (3) will now be expressed in the time domain. By use of Eq. (6) and inverse Fourier transformation, the time-domain equivalent of Eq. (5) can be expressed as the convolution of the impulse response and the input voltage of the amplifier, i.e.,

$$U_s(t) = \omega_{\text{cut}} G^0 \int_0^t U(\tau) \mathrm{e}^{-\omega_{\text{cut}}(t-\tau)}\, \mathrm{d}\tau, \tag{9}$$

where it has been assumed that $U(t) = 0$ for $t < 0$. Substituting Eqs. (1) into Eq. (4) and the result into Eq. (2), one obtains

$$\left[1 - \frac{Z_1 - Z_{\text{ch}}^M}{Z_1 + Z_{\text{ch}}^M} \mathrm{e}^{-\mathrm{i}\omega t_{\text{tr}}}\right] \hat{i}_0(\omega) = 2(1 - k_a^2) C_a \left[1 - \frac{Z_1 - Z_{\text{ch}}^M}{Z_1 + Z_{\text{ch}}^M} \mathrm{e}^{-\mathrm{i}\omega t_{\text{tr}}}\right] \mathrm{i}\omega \hat{U}_0(\omega) + +8k_a^2 C_a K_a \frac{1}{Z_1 + Z_{\text{ch}}^M} [1 - \mathrm{e}^{-\mathrm{i}\omega t_{\text{tr}}}] \hat{U}_0(\omega), \tag{10}$$

where $t_{\text{tr}} = l/c$ is the wave transit time through the PBE. After inverse Fourier transformation, this relation gives the difference equation

$$\begin{aligned} i_0(t) = {} & \frac{Z_1 - Z_{\text{ch}}^M}{Z_1 + Z_{\text{ch}}^M} i_0(t - t_{\text{tr}}) + 2(1 - k_a^2) C_a \left[\frac{\mathrm{d}U_0}{\mathrm{d}t}(t) - \frac{Z_1 - Z_{\text{ch}}^M}{Z_1 + Z_{\text{ch}}^M} \frac{\mathrm{d}U_0}{\mathrm{d}t}(t - t_{\text{tr}})\right] \\ & + 8k_a^2 C_a K_a \frac{1}{Z_1 + Z_{\text{ch}}^M} [U_0(t) - U_0(t - t_{\text{tr}})] \end{aligned} \tag{11}$$

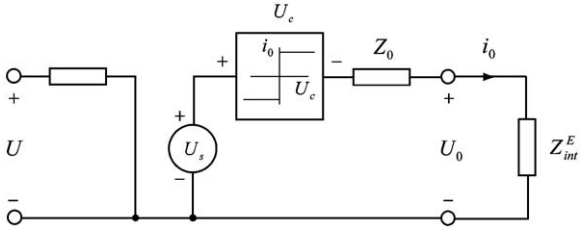

Fig. 2. Equivalent circuit of power amplifier with current constraint driving PBE–bar assembly.

for the output current, and, inversely, the difference-differential equation

$$\frac{dU_0}{dt}(t)+4\frac{k_a^2}{1-k_a^2}K_a\frac{1}{Z_1+Z_{ch}^M}U_0(t)=\frac{Z_1-Z_{ch}^M}{Z_1+Z_{ch}^M}\frac{dU_0}{dt}(t-t_{tr})+4\frac{k_a^2}{1-k_a^2}K_a\frac{1}{Z_1+Z_{ch}^M}U_0(t-t_{tr})+\frac{1}{2(1-k_a^2)C_a}\left[i_0(t)-\frac{Z_1-Z_{ch}^M}{Z_1+Z_{ch}^M}i_0(t-t_{tr})\right] \tag{12}$$

for the output voltage. Similarly, substitution of Eqs. (1) into Eq. (3) gives the relation

$$\left[1-\frac{Z_1-Z_{ch}^M}{Z_1+Z_{ch}^M}e^{-i\omega t_{tr}}\right]\hat{e}_G(\omega)=2\frac{A_aE_a}{AE}\frac{d_a}{h_a}\frac{Z_1}{Z_1+Z_{ch}^M}[1-e^{-i\omega t_{tr}}]\hat{U}_0(\omega), \tag{13}$$

which after inverse Fourier transformation results in the difference equation for the strain

$$e_G(t)=\frac{Z_1-Z_{ch}^M}{Z_1+Z_{ch}^M}e_G(t-t_{tr})+2\frac{A_aE_a}{AE}\frac{d_a}{h_a}\frac{Z_1}{Z_1+Z_{ch}^M}[U_0(t)-U_0(t-t_{tr})]. \tag{14}$$

The process of wave generation starts in the linear regime, $i_{min}<i_0(t)<i_{max}$. Initially, therefore, the output voltage $U_0(t)$ is obtained from Eqs. (7) and (9), and the output current $i_0(t)$ is obtained from $U_0(t)$ by use of Eq. (11). If at some instant of time $i_0(t)$ becomes equal to i_{max} or i_{min}, there is a transition into the current-constrained regime. From this time, the output voltage $U_0(t)$, subject to the requirement of continuity, is obtained by solving the difference-differential Eq. (12) with $i_0(t)=i_{max}$ or i_{min}. The voltage $U_c(t)$ is obtained from $U_0(t)$ and $U_s(t)$ by use of Eqs. (8) and (9). If at some instant of time $U_c(t)$ becomes zero, there is a transition back into the linear regime. By this procedure, the output voltage $U_0(t)$ can be determined for $t>0$. The strain $e_G(t)$ at the PBE–bar interfaces is obtained in terms of $U_0(t)$ by solving the difference Eq. (14), and at a distance a outside the PBE–bar interfaces, the strain is $e(t)=e_G(t-a/c_1)$.

6. Experiment

The experimental set-up, shown in Fig. 3, was the same as the one described in Ref. [10]. A vertical aluminium bar, clamped at its upper end, was used. In order to accommodate the piezoelectric actuators, its cross-sectional dimensions $h_1=w_1=4.0\,\text{mm}$ were reduced to $h_c=1.02\,\text{mm}$, $w_c=4.0\,\text{mm}$ by symmetric milling along the full length $l=95.4\,\text{mm}$ of the PBE region. The material of the bar had Young's modulus $E_1=69\,\text{GPa}$, Poisson's ratio $\nu_1=0.3$ and density $\rho_1=2700\,\text{kg/m}^3$. The actuators, bonded to the bar with a thin layer of epoxy adhesive, were of ceramic type and had cross-sectional dimensions $h_a=0.66\,\text{mm}$ and $w_a=6.4\,\text{mm}$. The piezoelectric material had closed-circuit Young's modulus $E_a=66\,\text{GPa}$, density $\rho_a=7800\,\text{kg/m}^3$, permittivity $\varepsilon_a=1.6\times10^{-8}\,\text{A s/V m}$, and piezoelectric constant $d_a=-d_{31}=190\times10^{-12}\,\text{m/V}$. At a distance of $a=800\,\text{mm}$ from the lower end of the PBE, the bar was instrumented with three semiconductor strain gauges, two with axial orientation opposite to each other and one with transverse orientation. The PBE and the strain gauges were surrounded by Faraday cages, grounded together with the bar. Each strain gauge was connected to a bridge amplifier with bandwidth 100 kHz (3 dB).

The dimensions and material properties of the PBE–bar assembly correspond to wave speed $c_1=5050\,\text{m/s}$ in the bar and $c=3300\,\text{m/s}$ in the PBE, wave transit time through the PBE $t_{tr}=28.9\,\mu\text{s}$, characteristic impedance $Z_1=219\,\text{N s/m}$ in

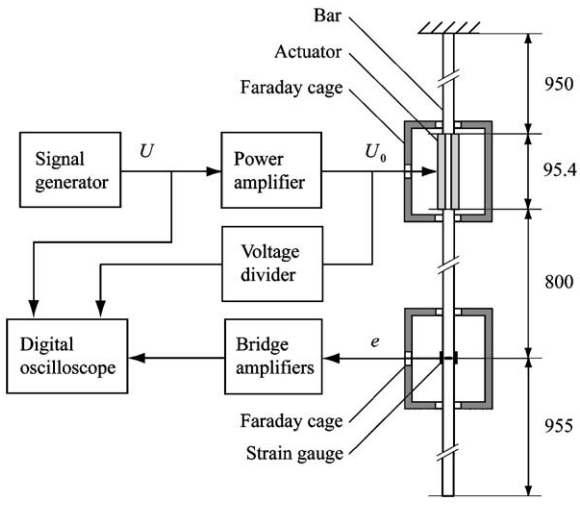

Fig. 3. Experimental set-up.

the bar and $Z_{\mathrm{ch}}^{M} = 254\,\mathrm{N\,s/m}$ in the PBE, capacitance of the unloaded actuator $C_a = 14.7\,\mathrm{nF}$, and piezoelectric coupling coefficient $k_a^2 = 0.150$.

The actuators were driven in phase by a power amplifier with input from a signal generation card. The amplifier had specified current constraints $\pm 200\,\mathrm{mA}$ and the following properties obtained from identification tests [10]: output impedance $Z_0 = R_0 + \mathrm{i}\omega L_0$ with $R_0 = 81\,\Omega$ and $L_0 = 2.4\,\mu\mathrm{H}$; 3 dB cut-off frequency 82 kHz.

Before there was any influence of reflected waves from the ends of the bar, the three strains, and the input and output voltages of the power amplifier were recorded with a sampling rate of 10 MHz by means of a digital oscilloscope card. The axial strain $e(t)$ was obtained by combining the recorded strains so that disturbances from unintended bending and electromagnetic noise from the actuators were suppressed [10].

Two tests were run at room temperature with DC-gain G^0 approximately 12. Step voltages were chosen as input of the power amplifier. The results for a 9 V step will be presented and discussed below.

7. Results and discussion

The spectra of the experimental strain pulses had significant frequencies up to about 100 kHz, corresponding to wavelengths larger than about 51 mm in the bar and 33 mm in the PBE. These wavelengths, much larger than the corresponding transverse dimensions, justify the 1D model used.

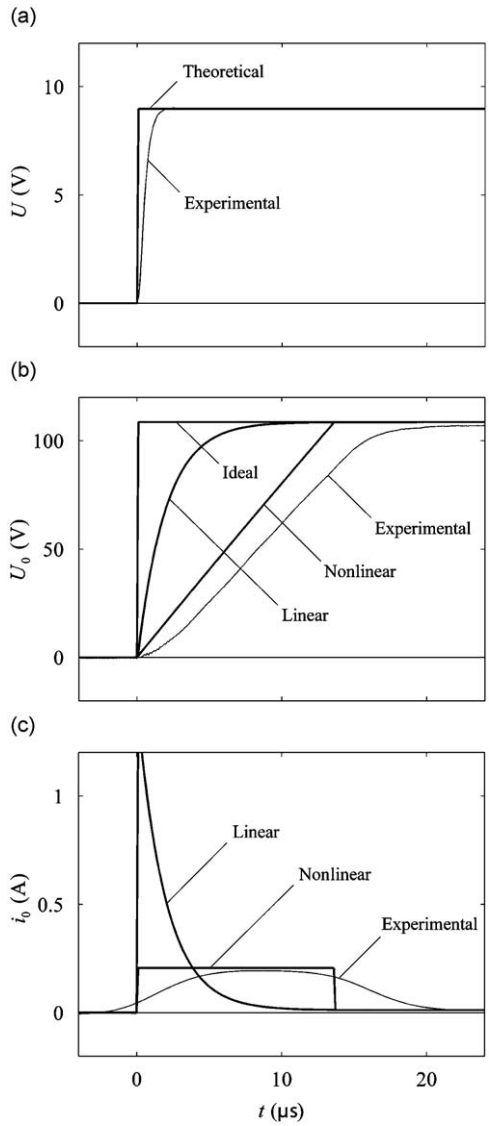

Fig. 4. Experimental results for voltage and current and corresponding theoretical results for ideal, linear and nonlinear model of the amplifier: (a) input voltage U; (b) output voltage U_0; and (c) output current i_0 versus time t.

The theoretical results for the output voltage, the output current and the strain associated with the generated waves are based on a three-level hierarchy of amplifier models: (i) the *nonlinear* amplifier model is the one defined by Eqs. (5)–(8); (ii) the *linear* amplifier model is obtained from the nonlinear one by removing its current constraints ($i_{\min}$and $i_{\max}$ infinite); and (iii) the *ideal* amplifier model, finally, is obtained from the linear one by taking ω_{cut} as infinite. Furthermore, the theoretical results are based on the theoretical input voltage to the amplifier. As shown in Fig. 4(a), this is a Heaviside step function with amplitude $U_{\max} = 9\,\text{V}$, while the experimental input voltage has the same amplitude but rise time of the order of a microsecond. This difference between the theoretical and experimental input gives rise to corresponding differences between the theoretical and experimental output.

The results for output voltage and current from the amplifier are shown in Fig. 4(b) and (c), respectively. The experimental result for output current was obtained from the experimental output voltage by use of Eq. (11), and a second-order Butterworth filter with cut-off frequency 100 kHz in order to remove noise. The results show that the nonlinear amplifier model is significantly more accurate than the linear model which, in turn, is significantly more accurate than the ideal amplifier model. For times of the order of the rise time of the output voltage, the nonlinear amplifier model gives results that reasonably agree, whereas the linear and ideal amplifier models give results that significantly disagree, with the experimental results. For times much smaller than the rise time of the output voltage, the amplifier models are all inaccurate, while for times much larger than this rise time they are all accurate.

The experimental and theoretical results show that the amplifier enters the current-constrained regime shortly after the input step voltage has been applied. This is explained by the capacitive nature of the internal impedance of the PBE–bar assembly which can be approximated as $Z^E_{\text{int}} \approx 1/\text{i}\omega C$ with $C \approx 2(1-k_a^2)C_a = 25.1\,\text{nF}$ [9]. With this approximation, the output current $i_0 \approx C\,\text{d}U_0/\text{d}t$ quickly reaches its upper limit $i_{\max}$ so that the rate of increase of the output voltage becomes almost constant, $\text{d}U_0/\text{d}t \approx i_{\max}/C = 8.0\,\text{V}/\mu\text{s}$. Theoretically, the amplifier returns into its linear regime when the voltage U_c defined by Eq. (8) becomes zero, i.e., when the nonlinear result $U_0 \approx (i_{\max}/C)t$ for the output voltage coincides with the corresponding linear result $U_0 = U_s$ given by Eq. (7). If the dynamics of the amplifier is neglected, $U_s \approx G^0 U_{\max}$. Therefore, the duration t_c of current-constrained operation can be estimated as $t_c \approx CG^0 U_{\max}/i_{\max} = 13.5\,\mu\text{s}$. This agrees well with the nonlinear result $t_c = 13.6\,\mu\text{s}$ in Fig. 4(b). For subsequent times, when the amplifier operates linearly, the nonlinear and linear results for the output voltage remain the same in agreement with Eq. (7).

The nonlinear rate of increase of the output voltage, $\text{d}U_0/\text{d}t = 8.0\,\text{V}/\mu\text{s}$, in perfect agreement with the estimation above, is slightly higher than the experimental rate at the inflection point, 7.2 V/μs. According to the relation $\text{d}U_0/\text{d}t \approx i_{\max}/C$, the higher nonlinear rate may correspond to a capacitance C that is too low or a current constraint $i_{\max}$ that is too high. In the former case, the experimental output current, evaluated from the experimental output voltage by use of Eq. (11), which can be approximated by $i_0 \approx C\,\text{d}U_0/\text{d}t$, would be too low. This is consistent with Fig. 4(c) which shows that the maximum experimental output current of the amplifier is somewhat lower than the upper current constraint. The linear rate, 43 V/μs, is considerably higher than the experimental rate, and the ideal rate is infinite. The delay of about a microsecond of the experimental rise relative to the nonlinear rise of the output voltage may be partially due the finite rise time of similar magnitude of the experimental input voltage.

The results for strain in the bar e associated with the waves generated are shown in Fig. 5. They consist of a main pulse followed by a tail formed by reflections of waves between the PBE–bar interfaces, at which there is a mismatch between the characteristic impedances $Z^M_{\text{ch}} = 254\,\text{N s/m}$ of the PBE and $Z_1 = 219\,\text{N s/m}$ of the bar. The width of the ideal main pulse is equal to the transit time $t_{\text{tr}} = 28.9\,\mu\text{s}$ for a wave through the PBE, and those of the linear, nonlinear and experimental pulses approximately agree with this result. The amplitude of the experimental pulse is somewhat lower than that predicted by theory, similarly as in Ref. [10]. A possible reason is that the effects of transverse strains were neglected in both studies. Overall, however, there is a fair agreement between the nonlinear and experimental strain pulses, while the linear and ideal strain pulses significantly differ from those obtained experimentally.

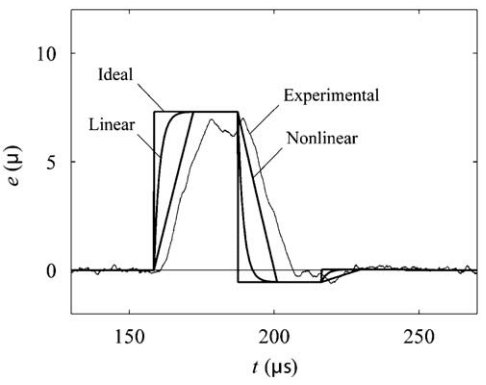

Fig. 5. Experimental result for strain wave generated and corresponding theoretical results for ideal, linear and nonlinear amplifier. Axial strain e at instrumented bar section versus time t.

8. Conclusions

Nonlinearity due to constrained amplifier output current strongly affects the response of actuator and structure to a given input voltage of the amplifier. The suggested amplifier model allows prediction of the main features of the nonlinear response in the output voltage, the output current, and the strains associated with the waves generated. Undesirable, nonlinear operation due constrained output current is not exceptional; due to the capacitive nature of the input impedance of the PBE–bar assembly, this phenomenon may occur even at low input voltage if the rate of change of this voltage is excessive. Therefore, it is important, e.g., in control applications, to take into consideration the effects of nonlinearity caused by constrained output current.

Acknowledgement

The Authors gratefully acknowledge economical support from the Swedish Research Council (Contract no 621-2001-2156).

References

[1] P. Nauclér, B. Lundberg, T. Söderström, A mechanical wave diode: using feedforward control for one-way transmission of elastic extensional waves, *IEEE Transactions on Control Systems Technology* 15 (4) (2007).
[2] E.F. Crawley, J. de Luis, Use of piezoelectric actuators as elements of intelligent structures, *AIAA Journal* 25 (10) (1987) 1373–1385.
[3] J. Pan, C.H. Hansen, S.D. Snyder, A study of the response of a simply supported beam to excitation by a piezoelectric actuator, *Journal of Intelligent Material Systems and Structures* 3 (1) (1992) 3–16.
[4] N.W. Hagood, W.H. Chung, A. von Flotow, Modelling of piezoelectric actuator dynamics for active structural control, *Journal of Intelligent Material Systems and Structures* 1 (3) (1990) 327–354.
[5] R.P. Thornburgh, A. Chattopadhyay, Simultaneous modeling of mechanical and electrical response of smart composite structures, *AIAA Journal* 40 (8) (2002) 1603–1610.
[6] R.P. Thornburgh, A. Chattopadhyay, A. Ghoshal, Transient vibration of smart structures using a coupled piezoelectric-mechanical theory, *Journal of Sound and Vibration* 274 (2004) 53–72.
[7] C. Niezrecki, H.H. Cudney, Improving the power consumption characteristics of piezoelectric actuators, *Journal of Intelligent Material Systems and Structures* 5 (1994) 522–529.
[8] D.J. Leo, Energy analysis of piezoelectric-actuated structures driven by linear amplifiers, *Journal of Intelligent Material Systems and Structures* 10 (1) (1999) 36–45.
[9] A. Jansson, B. Lundberg, Piezoelectric generation of extensional waves in a viscoelastic bar by use of a linear power amplifier: theoretical basis, *Journal of Sound and Vibration* 306 (2007) 318–332.
[10] A. Jansson, U. Valdek, B. Lundberg, Generation of prescribed waves in an elastic bar by use of piezoelectric actuators driven by a linear power amplifier, *Journal of Sound and Vibration* 306 (2007) 751–765.
[11] A. Jansson, B. Lundberg, Three-port impedance model of a piezoelectric bar element: application to generation and damping of extensional waves, *Journal of Sound and Vibration* 315 (2008) 985–1002.